J. Cell. Mol. Med. Vol 16, No 12, 2012 pp. 2925-2934

Diabetes influences cardiac extracellular matrix remodelling after myocardial infarction and subsequent development of cardiac dysfunction

Megumi Eguchi [a, b], Guoxiong Xu [b, c], Ren-Ke Li [d], Gary Sweeney [a, b, *]

[a] *Department of Biology, York University, Toronto, ON, Canada*
[b] *Institut Pasteur Korea, Seoul, South Korea*
[c] *Jinshan Hospital, Fudan University, Shanghai, China*
[d] *Division of Cardiovascular Surgery and Toronto General Research Institute, University Health Network and Department of Surgery, Division of Cardiac Surgery, University of Toronto, ON, Canada*

Received: April 11, 2012; Accepted: August 1, 2012

Abstract

This study was conducted to examine the influence of acute streptozotocin-induced diabetes on cardiac remodelling and function in mice subjected to myocardial infarction (MI) by coronary artery ligation. Echocardiography analysis indicated that diabetes induced deleterious cardiac functional changes as demonstrated by the negative differences of ejection fraction, fractional shortening, stroke volume, cardiac output and left ventricular volume 24 hrs after MI. Temporal analysis for up to 2 weeks after MI showed higher mortality in diabetic animals because of cardiac wall rupture. To examine extracellular matrix remodelling, we used fluorescent molecular tomography to conduct temporal studies and observed that total matrix metalloproteinase (MMP) activity in hearts was higher in diabetic animals at 7 and 14 days after MI, which correlated well with the degree of collagen deposition in the infarct area visualized by scanning electron microscopy. Gene arrays indicated temporal changes in expression of distinct MMP isoforms after 1 or 2 weeks after MI, particularly in diabetic mice. Temporal changes in cardiac performance were observed, with a trend of exaggerated dysfunction in diabetic mice up to 14 days after MI. Decreased radial and longitudinal systolic and diastolic strain rates were observed over 14 days after MI, and there was a trend towards altered strain rates in diabetic mouse hearts with dyssynchronous wall motion clearly evident. This correlated with increased collagen deposition in remote areas of these infarcted hearts indicated by Masson's trichrome staining. In summary, temporal changes in extracellular matrix remodelling correlated with exaggerated cardiac dysfunction in diabetic mice after MI.

Keywords: diabetes • myocardial infarction • extracellular matrix • collagen • fibrosis • matrix metalloproteinase • cardiac function

Introduction

It is well-established that diabetes confers an elevated risk of cardiovascular disease, including heart failure [1, 2]. Moreover, diabetes is confirmed as an independent risk factor for the development of heart failure after initial MI [3, 4], and it has been proposed that diabetes elevates the mortality caused by heart disease by 2–4 times [1]. The incidence of MI and subsequent events is dictated by numerous cardiac remodelling events [5]. Diabetes not only increases the incidence of initial MI but also the rate and the degree of cardiac remodelling events that take place after MI [6]. Nevertheless, precisely how diabetes impacts upon cardiac remodelling after MI remains to be conclusively established.

One important remodelling event involves changes in the synthesis and degradation of the cardiac extracellular matrix (ECM) [7, 8]. A normal, well-ordered collagen network plays important roles in cardiac function as a structural support and in providing elasticity, but the progressive loss of this network and subsequent fibrosis are clearly detrimental [9]. MI-induced cardiac remodelling is associated with a robust activation of matrix metalloproteinases, which degrade collagen. Numerous studies using both transgenic animals and pharmacological inhibitors have demonstrated that altered activity of matrix metalloproteinases in the heart is associated with adverse cardiac remodelling [10–14]. Importantly, a large number of matrix

*Correspondence to: Gary SWEENEY,
Department of Biology, York University, Toronto,
Ontario, Canada M3J 1P3
Tel.: +(1) 416-736-2100 (ext. 66635)
Fax: +416-736-5698
E-mail: gsweeney@yorku.ca

doi: 10.1111/j.1582-4934.2012.01613.x

metalloproteinase isoforms are expressed in the heart, and they have been reported to be activated in different regions of the heart at different times after MI [15]. Excessive activation of matrix metalloproteinases in the infarct area after MI causes a reduction in the collagen cross-linking network, resulting in cardiac rupture [11, 16, 17]. Excessive degradation of the ECM is also known to be associated with thinning of the cardiac wall as well as accelerated slippage of cardiomyocytes and dilation of the left ventricle [18–20].

This study was designed to investigate the influence of diabetes, induced by acute streptozotocin administration, on temporal changes in cardiac remodelling and function after ischaemic injury. In particular, our work focused on ECM remodelling by studying matrix metalloproteinase expression and activation, collagen synthesis and structure and the consequent development of cardiac dysfunction.

Materials and methods

Generation of diabetic mice and induction of MI

Diabetes was induced in male C57BL6 mice (aged 8–10 weeks) *via* a single-dose intraperitoneal injection of 150 mg/kg streptozotocin (STZ; Sigma-Aldrich, St. Louis, MO, USA) in 0.1 M citrate buffer, pH 4.1 [21]. Animals were confirmed as diabetic when the blood glucose level reached > 300 mg/dl, 4 days after the STZ administration (STZ animals). Control animals received the citrate buffer only as vehicle (VEH) treatment. Four days after injection of STZ, blood glucose levels in animals were tested and found to be 142.14 ± 5.88 mg/dl in VEH-injected and 514.06 ± 14.84 mg/dl in STZ-injected mice. These animals were randomly separated into sham and MI groups and MI was induced in the MI animals as previously described [22]. The sham animals underwent the same procedure except for the ligation of the suture around the coronary artery. To induce MI, the ligation was made at 2 mm below the tip of the left atrium, resulting in an infarct area of ~30–40% of the left ventricle. The heart samples were collected post mortem after spontaneous death or killed on days 1, 3, 7 and 14 after MI. After the surgery, all dead animals were subjected to autopsy, and cardiac rupture was confirmed by the presence of blood pool in the chest cavity. The Animal Care Committee of Institut Pasteur Korea approved all experimental procedures described below, which were carried out according to the Guide for the Care and Use of Laboratory Animals (NIH, publication No. 86-23, revised 1996).

Masson's trichrome staining and infarct area calculation

Infarct area was examined by staining heart sections with the standard Masson's trichrome method as previously described [23]. Seven 5 μm sections of frozen heart isolated at days 3, 7 and 14 after MI were prepared from the top to the apex of the heart. Each stained section was scanned and quantified using ImageJ software (NIH, Bethesda, MD, USA). The infarct area was measured as the ratio (%) of the infarct area divided by the entire left ventricular (LV) area.

Echocardiography analysis

Images were obtained using the Vevo2100 (Visual Sonics, Toronto, ON, Canada) equipped with an MS550D transducer (Visual Sonics, Toronto, ON, Canada). The mice were lightly anaesthetized using 1.5% isofluorane mixed with 100% O_2 during the time of imaging. The images were obtained from the B-mode long-axis view and the M-mode of the parasternal short-axis view. All parameters were averaged over at least three cardiac cycles for analysis. Speckle-tracking cardiac strain analysis was performed with Vevostrain software (Visual Sonics, Toronto, ON, Canada) incorporated into the Vevo2100 from the movies acquired from the B-mode long-axis view. The tracking quality was visually inspected, and the tracing was confirmed as acceptable when the traced line moved along with the moving heart image for at least three cardiac cycles. These cardiac cycles were used for the analysis. Left ventricular end-diastolic diameter (LVEDd), end-systolic diameter (LVEDs), end-diastolic area (LVEAd) and end-systolic area (LVEAs) were measured. LV end-diastolic volume (LVEDV) and end-systolic volume (LVESV) were calculated using the following formulae: $LVEDV = 1.047 \times LVEDd^3$ and $LVESV = 1.047 \times LVEDs^3$. Per cent ejection fraction (%EF) and fractional area change (%FAC) of the LV were calculated as follows: $\%EF = [(LVEDV - LVESV)/LVEDV] \times 100$; $\%FAC = [(LVEAd - LVEAs)/LVEAd] \times 100$.

Matrix metalloproteinase activity analysis using fluorescent molecular tomography

The degree and site of matrix metalloproteinase activation in the heart was analysed *ex vivo* with an FMT system, Visen FMT2500, using the MMPSense680 probe (Perkin Elmer, Waltham, MA, USA). It is a near-infrared fluorescence agent activated by key matrix MMPs, including MMP2, −3, −9 and −13. The animals were anaesthetized with 3% isofluorane and injected with 0.1 nmol/g MMPSence680 *via* retro-orbital injection 24 hrs prior to excision of the heart and imaging. This technique allows the rapid visualization and quantification of matrix metalloproteinase activity. The heart was excited at 680 nm and the emission detected at 700 nm. Tomographic reconstruction extracted information based on the fluorescence signal and this was integrated into quantitative data using proprietary software (Perkin Elmer).

Scanning electron microscopy analysis of collagen structure

Samples for SEM were fixed in 2% glutaraldehyde in 0.1 M sodium cacodylate buffer pH 7.3 for at least 2 hrs, rinsed in the buffer and dehydrated in a graded ethanol series. The samples were critical point dried in a Bal-tec CPD030 (Bal Tec, Los Angeles, CA, USA) critical point dryer, mounted on aluminium stubs, gold coated in a Denton Desk II sputter coater and examined in an FEI XL30 SEM (Philips, Markham, ON, Canada). SEM analysis was then performed as fee for service by Mr. Douglas Holmyard from Mount Sinai Hospital, Pathology and Laboratory Medicine.

Gene arrays for determining expression of matrix metalloproteinase and tissue inhibitors of metalloproteinase isoforms

RNA was isolated using RNeasy Fibrous Tissue Mini Kit (Qiagen, Valencia, CA, USA) from the infarct area of heart samples, which were immediately immersed in RNAlater RNA stabilization reagent (Qiagen) after isolation from the animals. RNA quality was improved with RNeasy MinElute Cleanup Kit (Qiagen), and sample integrity was confirmed *via* OD 260/280 nm reading between 1.8 and 2.0. Equal amounts of RNA (0.8 μg) were reversed transcribed with RT^2 First Strand cDNA kit (SABiosciences, Frederick, MD, USA) and subsequently analysed for numerous ECM-related matrix metalloproteinase and TIMP genes in a customized PCR Array following manufacturer's instructions (SABiosciences), and analysed using PT^2 Profiler PCR Array Analysis software, version 3.4 (Qiagen, Valencia, CA, USA).

Statistical analysis

Comparison of survival rates between the VEH and STZ groups was performed by Kaplan–Meier analysis. All other data are expressed as the mean ± SEM and were analysed using *t*-test or one-way ANOVA followed by Tukey *post hoc* test, and differences were determined to be statistically significant when $P < 0.05$. Gene array analysis was performed following manufacturers' instructions and using software provided from SABioscence for this purpose. The data presented represent a mean of delta–delta Ct, which is based on a 95% confidence interval between comparisons.

Results

Cardiac function was first assessed 1 day after MI by echocardiography. The negative percentage change in ejection fraction, fractional shortening and stroke volume were significantly larger in STZ-treated mice compared with the VEH-treated control mice demonstrating a worsen cardiac dysfunction induced by diabetes (Fig. 1, $*P < 0.05$). It should also be noted that STZ-treated mice had a lower heart rate. Although the MI resulted in ventricular dilation in control mice, the net change in end-diastolic and end-systolic left ventricular (LV) volumes were significantly greater in STZ-treated mice compared with the VEH-treated control mice (Fig. 1, $*P < 0.05$). These data suggest that diabetes accelerated progressive ventricular dilation.

Kaplan–Meier survival analysis indicated that the mortality rate of STZ mice after MI was significantly higher than that in the VEH mice (Fig. 2A, $P < 0.05$). This was particularly noticeable at 1 week after infarction as the decline in the survival of VEH mice occurred principally within the first week after MI and stabilized afterwards, whereas the survival rate of STZ mice continued to decline until day 14 after MI (Fig. 2A). Post mortem analysis was performed on all animals and the presence of cardiac wall rupture was evident as cause of death. Analysis of the infarct area with Masson's trichrome staining suggested no significant change in the size of the infarct after MI between the groups (Fig. 2B). An apparent increase in collagen accumulation (blue staining) over time is evident in the infarct area of VEH hearts, but this was not observed in STZ hearts (Fig. 2B). The temporal extent and location of matrix metalloproteinase activation in the heart was analysed using fluorescent molecular tomography (FMT). A higher level of matrix metalloproteinase activity was observed in STZ mice, notably at 7 and 14 days after MI (Fig. 2C and

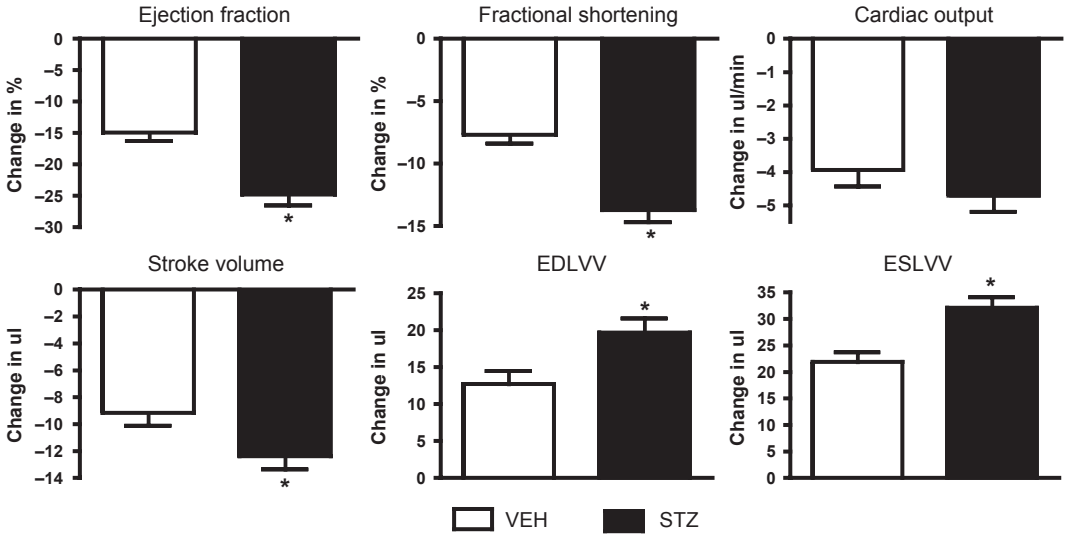

Fig. 1 Changes in cardiac functions 24 hrs after MI. Difference in echocardiographic measurements between sham and MI animals are shown for vehicle (VEH) animals (shown in white) and diabetic (STZ) animals (shown in black bar). $n \geq 4$/group. * indicates $P < 0.05$ *versus* its own sham group. EDLVV: end-diastolic left ventricular volume, ESLVV: end-systolic left ventricular volume.

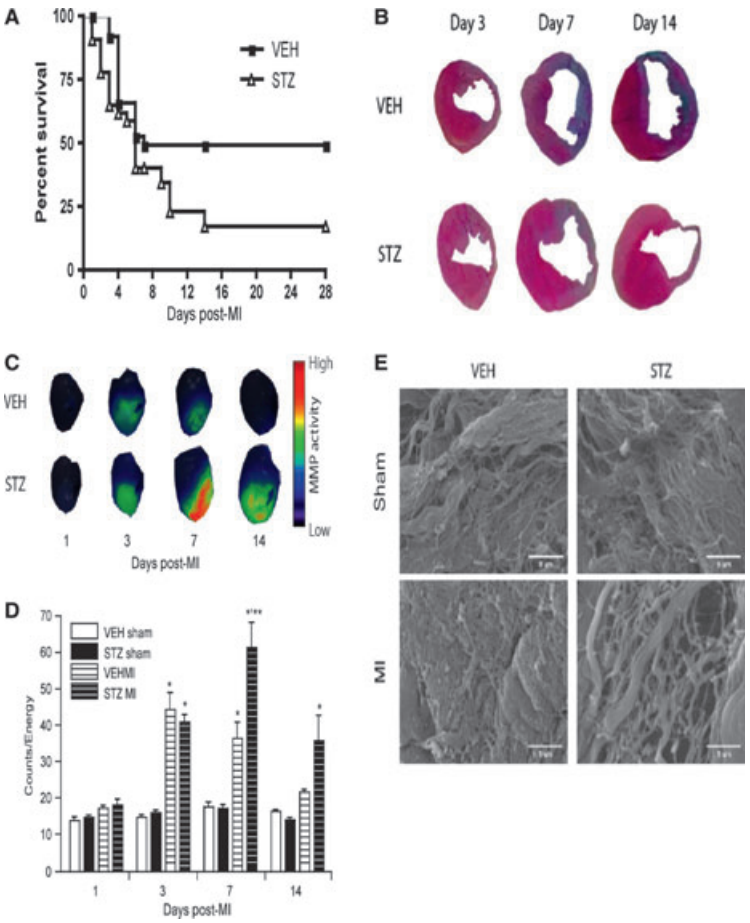

Fig. 2 ECM remodelling is enhanced in STZ mice after MI. (A) Kaplan–Meier analysis shows that the decline in the survival rate of VEH and STZ mice is similar up to day 7 after MI. The survival rate stops declining starting day 7 after MI in VEH mice, but the STZ mice continue to show a decline in survival rate up to day 14 after MI. The survival rate of the STZ animals is significantly lower compared with that of VEH mice ($P < 0.05$). (B) Masson's trichrome staining of the frozen heart sections for visualizing the infarct area indicate myocytes in red, collagen in blue and area with dead myocytes without collagen deposition in white. (C) Fluorescent molecular tomography (FMT) was used to assess the location and degree of matrix metalloproteinase activation in the heart after MI at different time-points. Representative FMT images for each treatment group at indicated times after MI. (D) Matrix metalloproteinase activity peaks on day 3 after MI in VEH hearts, whereas the peak is seen on day 7 in STZ hearts (*$P < 0.05$ *versus* sham, **$P < 0.05$ *versus* STZ). (E) Scanning electron microscope analysis demonstrates a disturbance in the fine collagen mesh network on day 7 after MI. The disturbance is much greater in STZ animals. Scale bars: 5 μm. $n \geq 3$/group.

D, *$P < 0.05$). This correlated well with the extent of collagen staining in the infarct area shown in Fig. 2B. In terms of localization, matrix metalloproteinase activation was predominately limited to the infarct area in both VEH and STZ hearts (Fig. 2C). We used scanning electron microscopy to study the collagen network structure in heart samples collected on day 7 after MI. Both VEH and STZ sham-operated hearts showed a healthy fine mesh-like collagen weave as expected (Fig. 2E). The infarcted VEH hearts exhibited an increase in the density of the collagen mesh composed of thin collagen filaments, whereas the infarcted STZ hearts showed a more disorganized collagen scaffold composed of numerous larger collagen fibres (Fig. 2E).

We used custom gene arrays to determine changes in the expression of various matrix metalloproteinase and TIMP isoforms that regulate collagen turnover. Figure 3A (1 week after MI) and 3F (2 weeks after MI) allow the comparison of these genes among all four groups, with the sham-operated VEH group acting as control in all cases. To clearly highlight up- or down-regulation of genes between individual groups, we have displayed direct 2-group analysis in Fig. 3B–E and G–J. MI in VEH mice induced expression of MMP2, −8, −9 and −14 at 1 week after MI (Fig. 3B) and MMP2, −3 and −14 at 2 weeks after MI (Fig. 3G). A decrease in TIMP4 expression was seen after 1 week (Fig. 3B), and increases in TIMP2 and three expressions were seen after 2 weeks (Fig. 3G). Diabetes alone induced a widespread

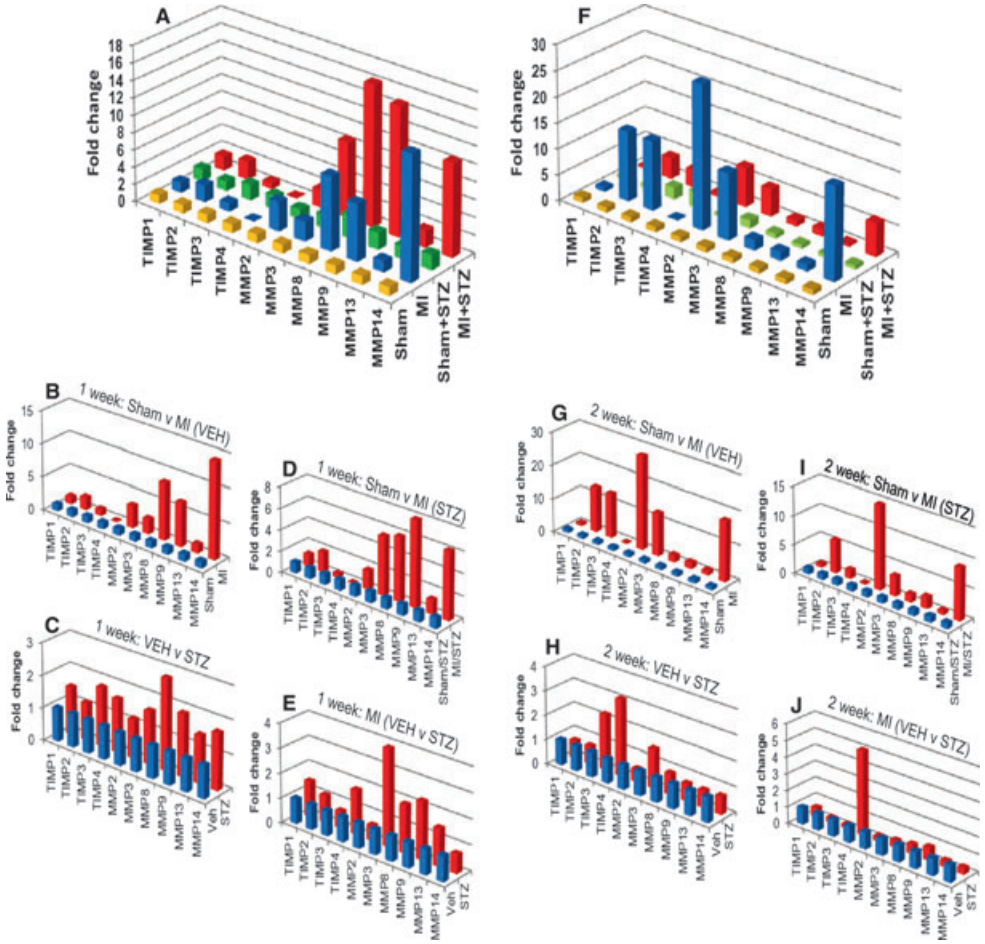

Fig. 3 Real-time PCR gene array. Fold changes at 1 week (A) and 2 weeks (F) after MI are shown with the sham-operated VEH group acting as control. The fold change in genes between individual groups is shown at 1 week (B–E) and 2 weeks (G–J) after MI. (B and G) Sham *versus* MI in VEH mice; (C and H) VEH *versus* STZ mice; (D and I) Sham *versus* MI in STZ mice; (E and J) MI in VEH *versus* STZ mice. $n > 3$ mice for each experimental group.

increase in matrix metalloproteinase and TIMP isoforms 1 week after MI (Fig. 3C), but, with the exception of TIMP3 and TIMP4, these genes returned to normal levels after 2 weeks (Fig. 3H). In the presence of diabetes, MI induced a similar pattern of gene expression changes as in non-diabetic mice (Fig. 3D and I), but with an overall greater magnitude of increase in matrix metalloproteinase gene expression at 1 week after MI (Fig. 3E) and a clear elevation of TIMP4 expression after 2 weeks (Fig. 3J).

Echocardiography analysis over 2 weeks following MI demonstrated the development of LV dilation in both VEH and STZ animals as indicated by an increase in end-diastolic (Fig. 4A) and end-systolic (Fig. 4B) LV volumes. These changes were apparent after 1 day and became progressively worse over time. Importantly, the degree of dilation was significantly greater in STZ animals compared with VEH animals (Fig. 4A and B, $*P < 0.05$). Temporal effects of diabetes on cardiac function after MI were assessed using fractional shortening (FS) (Fig. 4C) and cardiac output (CO) (Fig. 4D). Changes in FS after MI as a consequence of diabetes were maximal at day 1 and were maintained throughout the study period (Fig. 4C, $*P < 0.05$). Changes in CO, also manifested at 1 day, were maintained after 7 days, but returned to the same value as non-diabetic mice after 14 days (Fig. 4D, $*P < 0.05$). Ejection fraction values to indicate the heart function over the period of days 0–14 after MI were also assessed and can be summarized as follows: 38.2 ± 1.8, 38.2 ± 1.8, 27.9 ± 4.2 and 21.5 ± 7.5 in control mice at days 0, 1, 7 and 14 respectively. Corresponding values at these time-points in STZ mice were 50.9 ± 2.9, 26.1 ± 2.1, 32.8 ± 3.1 and 27.2 ± 4.1.

Speckle-tracking echocardiography analysis was used to provide a detailed analysis of changes in cardiac performance. At 14 days after MI, we observed that MI decreased radial and longitudinal systolic and diastolic strain rates in both VEH- and STZ-treated mice, but there was no significant difference between two groups (Fig. 5A and B, $*P < 0.05$ *versus* sham). LV synchronicity was examined by an established method of calculating the wall delay [24, 25]. This analysis divides the heart into

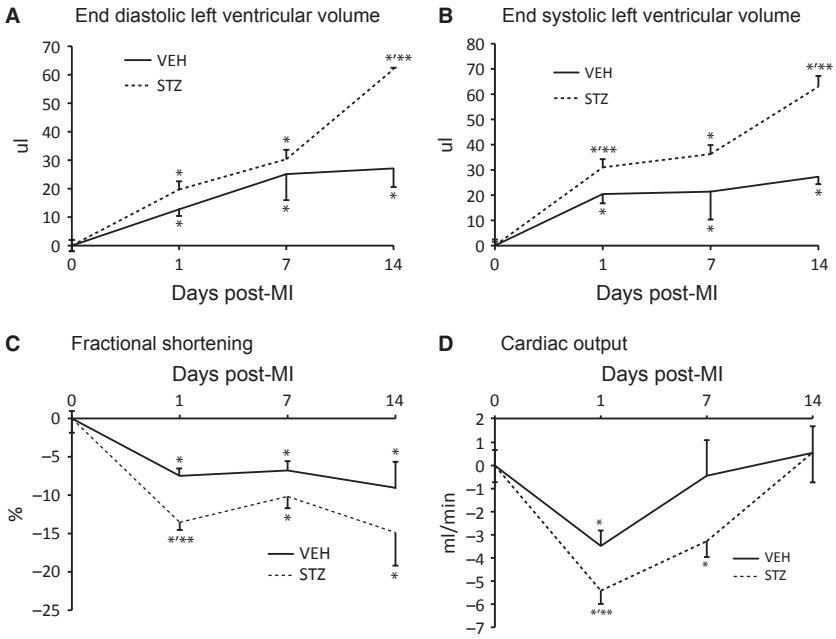

Fig. 4 Changes in cardiac structure and functions after MI compared with sham control. Both VEH and STZ animals develop LV dilation after MI as indicated by an increase in end-diastolic LV volume (A) and end-systolic LV volume (B). The degree of LV dilation is more severe in STZ animals. MI also leads to a decrease in fractional shortening over time (C). Cardiac output is initially decreased, but returns to normal by day 14 after MI (D). All graphs show the change compared with the sham control of each treatment group. $n \geq 3$/group/time-point. * indicates $P < 0.05$ *versus* its own sham group. ** indicates $P < 0.05$ *versus* VEH MI.

six separate segments (basal, mid and apex from the posterior and anterior walls) and calculates the difference in the time it takes for each segment of the heart to reach its peak strain. Results showed that wall delay increased after MI, and diastolic delay was significantly increased in STZ animals 14 days after MI demonstrating augmented LV dyssynchrony (Fig. 5C and D, $*P < 0.05$ *versus* sham, $**P < 0.05$ *versus* VEH). The representative images depicting wall delay are shown in Fig. 5E, and the patterns shown in Fig. 5F provide a clear visual example of dyssynchronous wall motion in the STZ mice 14 days after MI.

Wall motion is influenced by the degree of fibrosis; hence, we examined the amount of collagen accumulation in the area remote from the infarct by staining heart sections with Masson's trichrome. There was a small, but significant increase in collagen deposition in STZ hearts compared with VEH hearts at 7 and 14 days after MI (Fig. 6A and B).

Discussion

MI induces a complex series of remodelling events that involve a combination of initially compensatory changes, but which ultimately coalesce to bring heart failure [5, 26–28]. However, precisely how the presence of diabetes influences remodelling and cardiac function remains to be fully established. It is well-established from epidemiological and experimental data that diabetic patients or animal models have a higher propensity to develop severe cardiac dysfunction and also have a significantly higher mortality rate after the incident MI [2–4]. In this study we chose to use an acute period of diabetes induced by single injection of streptozotocin [29] to examine the influence on cardiac remodelling and function after MI induced by ligation of the left descending coronary artery [22].

Cardiac function and LV dimensions were evaluated using serial echocardiography. We found that diabetic mice had significantly impaired cardiac function after MI. This effect was associated with greater decrease in ejection fraction, fractional shortening, stroke volume and with increased ventricular dilatation in the STZ recipients relative to the vehicle controls. These data were in agreement with previously published studies regarding the cardiac dysfunction in experimental small and large animal diabetes after MI [30, 31]. These changes did not manifest in significant changes in cardiac output, likely owing to the fact that ventricular size of STZ animals was greater and the STZ mice had a lower heart rate. Nevertheless, overall changes in cardiac function induced by MI is clearly exacerbated in the STZ mice.

An extremely important component of LV remodelling leading to the progression of heart failure involves the reorganization of the cardiac ECM [7, 8, 32]. In human beings, various forms of heart failure are associated with distinct patterns of changes in matrix metalloproteinase and collagen isoforms, although all ultimately manifest as fibrosis [33–35]. Our current study indicated that STZ animals suffer from enhanced and accelerated LV remodelling after MI. The first and most apparent evidence for this was a higher mortality rate, which by observation was found to be mostly caused by cardiac wall rupture. We used scanning electron microscopy to examine changes in collagen networks [36, 37]. The changes observed were higher accumulation of collagen in the infarct area of VEH animals. The VEH hearts also demonstrated a better organization of the reconstructed collagen scaffold and formation of a mature scar in the infarct area by 1 week after MI. A further increase in the mortality rate seen in the STZ animals may have been caused by an intense degradation of collagen scaffold holding the ventricular wall intact and an abrogated formation of scar in the infarct area. The STZ animals also demonstrated a

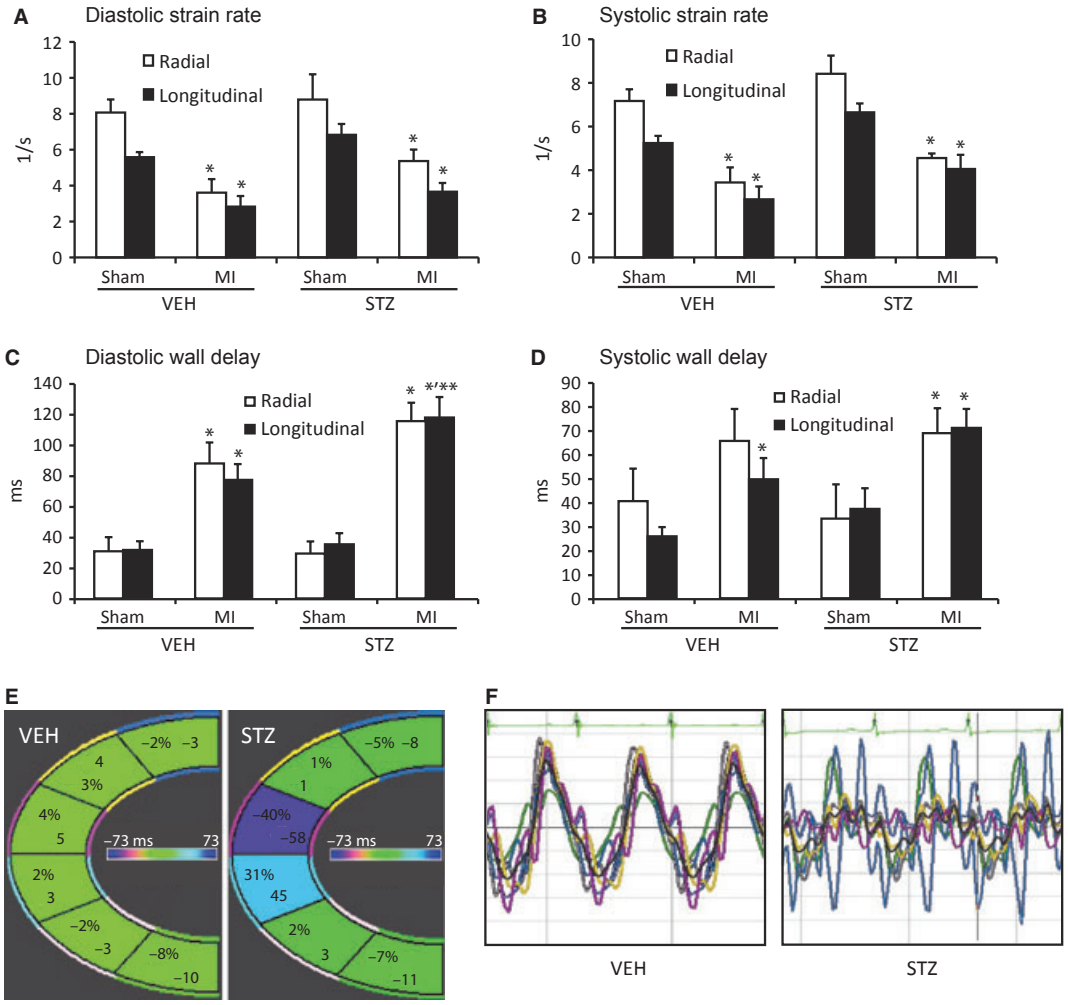

Fig. 5 Cardiac function measured on day 14 after MI. Both diastolic (A) and systolic (B) strain rates are reduced in VEH and STZ hearts on day 14 after MI. MI causes the heart to develop radial and longitudinal dyssynchrony during diastole (C) and systole (D). (E) The colour-coded images depicting the LV divided into six sectors indicate that the degree of cardiac dyssynchrony is greater in STZ hearts. The numbers in each LV sector indicate the difference in time between the peak strain rate of each sector to the average peak strain rate. This information is also displayed in percentage from −50 to +50. The dyssynchonic movement of the STZ heart is also demonstrated in (F), where the ununiform movement of each sector is clearly demonstrated. The colours on the graphs correspond to the colours of the sectors indicated on the pericardial portion in (E). $n \geq 3$/group/time-point. * indicates $P < 0.05$ *versus* its own sham group. ** indicates $P < 0.05$ *versus* VEH MI.

higher matrix metalloproteinase activity for a longer duration of time, and this may have contributed to the delay in mature scar formation.

We also observed exaggerated dilation of the left ventricle in diabetic mice after MI. Interestingly, it has been reported that the loss of collagen fibroskeleton is associated not only with cardiac rupture but also with myocyte slippage leading to the dilation of the LV [18–20]. In this study, both VEH and STZ hearts developed LV dilation as shown by an increase in endocardial volume during diastole and systole, but the degree of LV dilation was much more severe in STZ hearts. Again, a greater degree of collagen network decomposition seen in the STZ-diabetic heart without formation of a thick mature scar may be in part responsible for the greater progression of LV chamber dilation. Another reason leading to an intensive dilation of the LV in STZ heart is that these animals also exhibited a greater decrease in FS and cardiac output on day 1 after MI. The LV dilation is known to be initially a compensating mechanism of the heart to volume overload caused by MI to sustain a normal CO [15]. Indeed, the initial significant decrease in CO observed on day 1 after MI was brought back to the normal level by day 14 in both VEH and STZ animals. LV dilation most likely contributed to the compensated increase in CO, and STZ hearts may have compensated for the greater decrease in cardiac output by a greater dilation of the LV.

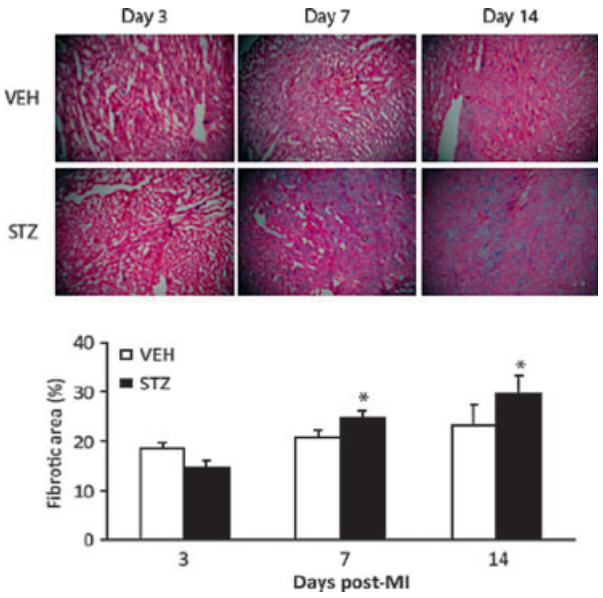

Fig. 6 Collagen deposition in the remote area after MI. (A) Representative images from each treatment group after MI. (B) Quantification of Masson's trichome staining indicated that STZ hearts exhibit a significant increase in the deposition of collagen in the remote area after MI. $n \geq 4$/group. * indicates $P < 0.05$ *versus* its own sham group.

A major driving force in collagen degradation and remodelling is changes in the expression and activity of matrix metalloproteinase and TIMP isoforms [36, 38]. Elevated activity of matrix metalloproteinase isoforms occurs after MI in a temporal and spatial manner, and various studies in animal models have shown that genetic deletion or pharmacological inhibition of matrix metalloproteinase prevents cardiac rupture or dysfunction after MI in mice [11, 39, 40]. Increased expression and activity of matrix metalloproteinase is well-established to occur in the infarcted heart, and overexpression of matrix metalloproteinase can exacerbate MI-induced dysfunction [13]. In our study we used fluorescent molecular tomography to examine cardiac matrix metalloproteinase activity in a temporal and spatial manner after MI in both VEH and STZ-diabetic mice. The latter showed elevated matrix metalloproteinase activity at 1 week after MI in the infarct area, and our gene expression analyses suggested this was correlated specifically with higher MMP3, −8, −9 and −13 levels after 1 week. It has been reported previously that increased matrix metalloproteinase activation is associated with the incidence of cardiac wall rupture [11, 41]. Prolonged degradation of the ECM contributes to the slippage of viable cells and wall thinning and with a very little ECM support, the heart is not able to resist the stress generated during pumping and the cardiac wall ruptures [36]. Cardiac wall rupture has been previously reported to occur within the first week after MI [11], consistent with the finding of our current study.

MI is known to induce fibrosis in the remote area of the heart over time [13], and this leads to detrimental effects on performance. We used speckle-tracking echocardiography to conduct cardiac strain analysis, allowing examination of the deformation of the LV wall and changes in overall LV contraction and relaxation in the mouse [24]. In agreement with previous work, this study also demonstrated that MI induces a reduction in the ability of the heart to deform as the heart contracts and dilates [24]. MI also caused the development of dyssynchronic cardiac wall motion in both VEH and STZ animals; however, STZ animals exhibited a greater disturbance in the synchronic motion of the cardiac wall. In the heart, a normal collagen fibroskeleton not only serves as the structural framework of the organ but also gives structural integrity to coordinate contraction of individual myocytes into overall heart contraction [7]. We suggest that the greater disturbance in the synchronic movement of the heart in diabetic animals may be caused by a greater remodelling of the ECM. This information has translational significance as it has also been reported previously that patients exhibiting a higher degree of cardiac fibrosis are more likely to develop cardiac dyssynchrony. Indeed, cardiac resynchronization therapy has been recently demonstrated to improve the function of the heart and survival in heart failure patients [25]. Notably, it would be interesting to further analyse the type of collagen deposition in the heart of these animals [7].

In summary, STZ mice exhibited a poorer outcome after MI. These mice showed a significantly higher activity of matrix metalloproteinase for an extended time period in the infarct area after MI. This was partly explained by an overall elevation in matrix metalloproteinase isoform expression in the infarct area. This was associated with a poor scar formation in the infarct area with an extensive degradation of the collagen skeletal framework. These hearts were more susceptible to cardiac wall rupture and subsequently higher mortality rate. These animals also exhibited a greater LV dilation with a greater disturbance in the synchronicity of movement of the heart, developing a severe cardiac dysfunction.

Acknowledgements

This work was funded by the Canadian Diabetes Association *via* a grant to G.S. M.E. was supported by a studentship from the Heart & Stroke Foundation of Canada.

Conflict of interest

No conflict of interest is declared by the authors.

References

1. **Roger VL, Go AS, Lloyd-Jones DM, *et al.*** Heart disease and stroke statistics–2011 update: a report from the American heart association. *Circulation*. 2011; 123: e18–209.
2. **Voors AA, van der Horst IC.** Diabetes: a driver for heart failure. *Heart*. 2011; 97: 774–80.
3. **Marma AK, Lloyd-Jones DM.** Systematic examination of the updated Framingham heart study general cardiovascular risk profile. *Circulation*. 2009; 120: 384–90.
4. **Preis SR, Hwang SJ, Coady S, *et al.*** Trends in all-cause and cardiovascular disease mortality among women and men with and without diabetes mellitus in the Framingham heart study, 1950 to 2005. *Circulation*. 2009; 119: 1728–35.
5. **Abel ED, Litwin SE, Sweeney G.** Cardiac remodeling in obesity. *Physiol Rev*. 2008; 88: 389–419.
6. **Katayama T, Nakashima H, Takagi C, *et al.*** Clinical outcomes and left ventricular function in diabetic patients with acute myocardial infarction treated by primary coronary angioplasty. *Int Heart J*. 2005; 46: 607–18.
7. **Fedak PW, Verma S, Weisel RD, *et al.*** Cardiac remodeling and failure from molecules to man (part II). *Cardiovasc Pathol*. 2005; 14: 49–60.
8. **Fomovsky GM, Thomopoulos S, Holmes JW.** Contribution of extracellular matrix to the mechanical properties of the heart. *J Mol Cell Cardiol*. 2010; 48: 490–6.
9. **Collier P, Watson CJ, van Es MH, *et al.*** Getting to the heart of cardiac remodeling; how collagen subtypes may contribute to phenotype. *J Mol Cell Cardiol*. 2012; 52: 148–53
10. **Kandalam V, Basu R, Abraham T, *et al.*** TIMP2 deficiency accelerates adverse post-myocardial infarction remodeling because of enhanced MT1-MMP activity despite lack of MMP2 activation. *Circ Res*. 2010; 106: 796–808.
11. **Matsumura S, Iwanaga S, Mochizuki S, *et al.*** Targeted deletion or pharmacological inhibition of MMP-2 prevents cardiac rupture after myocardial infarction in mice. *J Clin Invest*. 2005; 115: 599–609.
12. **Spinale FG.** Matrix metalloproteinases: regulation and dysregulation in the failing heart. *Circ Res*. 2002; 90: 520–30.
13. **Spinale FG, Mukherjee R, Zavadzkas JA, *et al.*** Cardiac restricted overexpression of membrane type-1 matrix metalloproteinase causes adverse myocardial remodeling following myocardial infarction. *J Biol Chem*. 2010; 285: 30316–27.
14. **Koskivirta I, Kassiri Z, Rahkonen O, *et al.*** Mice with tissue inhibitor of metalloproteinases 4 (Timp4) deletion succumb to induced myocardial infarction but not to cardiac pressure overload. *J Biol Chem*. 2010; 285: 24487–93.
15. **Hutchinson KR, Stewart JA Jr, Lucchesi PA.** Extracellular matrix remodeling during the progression of volume overload-induced heart failure. *J Mol Cell Cardiol*. 2010; 48: 564–9.
16. **Creemers EE, Cleutjens JP, Smits JF, *et al.*** Matrix metalloproteinase inhibition after myocardial infarction: a new approach to prevent heart failure? *Circ Res*. 2001; 89: 201–10.
17. **Spinale FG, Coker ML, Krombach SR, *et al.*** Matrix metalloproteinase inhibition during the development of congestive heart failure: effects on left ventricular dimensions and function. *Circ Res*. 1999; 85: 364–76.
18. **D'Armiento J.** Matrix metalloproteinase disruption of the extracellular matrix and cardiac dysfunction. *Trends Cardiovasc Med*. 2002; 12: 97–101.
19. **Gao XM, Dilley RJ, Samuel CS, *et al.*** Lower risk of postinfarct rupture in mouse heart overexpressing beta 2-adrenergic receptors: importance of collagen content. *J Cardiovasc Pharmacol*. 2002; 40: 632–40.
20. **Ichihara S, Senbonmatsu T, Price E Jr, *et al.*** Targeted deletion of angiotensin II type 2 receptor caused cardiac rupture after acute myocardial infarction. *Circulation*. 2002; 106: 2244–9.
21. **Han B, Baliga R, Huang H, *et al.*** Decreased cardiac expression of vascular endothelial growth factor and redox imbalance in murine diabetic cardiomyopathy. *Am J Physiol Heart Circ Physiol*. 2009; 297: H829–35.
22. **Tarnavski O, McMullen JR, Schinke M, *et al.*** Mouse cardiac surgery: comprehensive techniques for the generation of mouse models of human diseases and their application for genomic studies. *Physiol Genomics*. 2004; 16: 349–60.
23. **Schwartz SM, Gordon D, Mosca RS, *et al.*** Collagen content in normal, pressure, and pressure-volume overloaded developing human hearts. *Am J Cardiol*. 1996; 77: 734–8.
24. **Gnyawali SC, Roy S, Driggs J, *et al.*** High-frequency high-resolution echocardiography: first evidence on non-invasive repeated measure of myocardial strain, contractility, and mitral regurgitation in the ischemia-reperfused murine heart. *J Vis Exp*. 2010; doi: 10.3791/1781
25. **Suffoletto MS, Dohi K, Cannesson M, *et al.*** Novel speckle-tracking radial strain from routine black-and-white echocardiographic images to quantify dyssynchrony and predict response to cardiac resynchronization therapy. *Circulation*. 2006; 113: 960–8.
26. **Jugdutt BI.** Aging and remodeling during healing of the wounded heart: current therapies and novel drug targets. *Curr Drug Targets*. 2008; 9: 325–44.
27. **Jugdutt BI.** Remodeling of the myocardium and potential targets in the collagen degradation and synthesis pathways. *Curr Drug Targets Cardiovasc Haematol Disord*. 2003; 3: 1–30.
28. **Jugdutt BI.** Ischemia/Infarction. *Heart Fail Clin*. 2012; 8: 43–51.
29. **Rayat GR, Rajotte RV, Lyon JG, *et al.*** Immunization with streptozotocin-treated NOD mouse islets inhibits the onset of autoimmune diabetes in NOD mice. *J Autoimmun*. 2003; 21: 11–5.
30. **Shiomi T, Tsutsui H, Ikeuchi M, *et al.*** Streptozotocin-induced hyperglycemia exacerbates left ventricular remodeling and failure after experimental myocardial infarction. *J Am Coll Cardiol*. 2003; 42: 165–72.
31. **Ruan W, Lu L, Zhang Q, *et al.*** Serial assessment of left ventricular remodeling and function by echo-tissue Doppler imaging after myocardial infarction in streptozotocin-induced diabetic swine. *J Am Soc Echocardiogr*. 2009; 22: 530–6.
32. **van den Borne SW, Diez J, Blankesteijn WM, *et al.*** Myocardial remodeling after infarction: the role of myofibroblasts. *Nat Rev Cardiol*. 2010; 7: 30–7.
33. **Ban CR, Twigg SM.** Fibrosis in diabetes complications: pathogenic mechanisms and circulating and urinary markers. *Vasc Health Risk Manag*. 2008; 4: 575–96.
34. **Querejeta R, Lopez B, Gonzalez A, *et al.*** Increased collagen type I synthesis in patients with heart failure of hypertensive origin: relation to myocardial fibrosis. *Circulation*. 2004; 110: 1263–8.
35. **Polyakova V, Loeffler I, Hein S, *et al.*** Fibrosis in endstage human heart failure: severe changes in collagen metabolism and MMP/TIMP profiles. *Int J Cardiol*. 2011; 151: 18–33.
36. **Spinale FG.** Myocardial matrix remodeling and the matrix metalloproteinases: influence on cardiac form and function. *Physiol Rev*. 2007; 87: 1285–342.

37. **Spinale FG, Coker ML, Thomas CV, *et al.*** Time-dependent changes in matrix metalloproteinase activity and expression during the progression of congestive heart failure: relation to ventricular and myocyte function. *Circ Res*. 1998; 82: 482–95.
38. **Gallagher GL, Jackson CJ, Hunyor SN.** Myocardial extracellular matrix remodeling in ischemic heart failure. *Front Biosci*. 2007; 12: 1410–9.
39. **Rohde LE, Ducharme A, Arroyo LH, *et al.*** Matrix metalloproteinase inhibition attenuates early left ventricular enlargement after experimental myocardial infarction in mice. *Circulation*. 1999; 99: 3063–70.
40. **Tyagi SC, Campbell SE, Reddy HK, *et al.*** Matrix metalloproteinase activity expression in infarcted, noninfarcted and dilated cardiomyopathic human hearts. *Mol Cell Biochem*. 1996; 155: 13–21.
41. **Arikawa M, Kakinuma Y, Handa T, *et al.*** Donepezil, anti-Alzheimer's disease drug, prevents cardiac rupture during acute phase of myocardial infarction in mice. *PLoS ONE*. 2011; 6: e20629.